Chemical Science

ROYAL SOCIETY OF CHEMISTRY

EDGE ARTICLE

View Article Online
View Journal | View Issue

Open Access Article. Published on 15 April 2025. Downloaded on 3/21/2026 8:32:00 AM.
This article is licensed under a Creative Commons Attribution-NonCommercial 3.0 Unported Licence.

Check for updates

Cite this: *Chem. Sci.*, 2025, **16**, 8959

All publication charges for this article have been paid for by the Royal Society of Chemistry

An investigative study of electrochemical induced fluorescence for fluorophores†

Daniel E. Hagness,[ab] Ying Yang,[ab] Yuanqing Ma,[a] Sumaya Ishtiaq,[a] Sanjun Fan,[ab] Richard D. Tilley *[ac] and J. Justin Gooding *[ab]

Understanding and controlling the fluorescence of dye molecules is essential for many applications especially in biological imaging. Electrochemical-induced modulation of fluorescence provides the capability to non-destructively control the fluorescent emission of fluorophores, allowing new avenues to exploit for fluorescence imaging. This paper reports on the investigation of electrochemical-induced fluorescence modulation, focusing on the effect of the fluorophore chemical structure and the buffer composition. Of the twelve fluorophores investigated, it was observed that any variations in the chemical structure results in differences in how the fluorescence is modulated with potential. Our results showed that different core fluorescent structures exhibited distinctive modulation behaviours, the oxazine fluorophore (ATTO 655) was stable in the non-fluorescent configuration causing a prolonged low signal and the coumarin fluorophore (ATTO 390) possessed low response. Certain trends observed are related to the impact of the chemical structure on the fluorescence modulation with potential. For example, the low fluorescence modulation with potential for ATTO 390 suggests that the presence of the electron withdrawing $-N^+R_3$ group facilitates significant modulation, while a lack of the $-N^+R_3$ group results in low modulation. The unique response of ATTO 655 suggested the element at the radical site can affect the stability of the radical- and leuco-states and influence the fluorescence modulation that occurs. Additionally, the results show that buffer additives, such as oxygen scavengers and triplet quenchers, affect the fluorescence modulation either by stabilising the non-fluorescent radical or leuco-fluorophore structure, or improving photon emission. The quantitative characterisation of electrochemical fluorescence modulation behaviours for various fluorophores provides a guideline for future application of the fluorophores for sensing or imaging based on their performances.

Received 18th February 2025
Accepted 10th April 2025

DOI: 10.1039/d5sc01265a

rsc.li/chemical-science

Introduction

Fluorescence microscopy[1,2] employs fluorescent molecules, such as fluorophores, fluorescent proteins, and quantum dots, to give high quality images of biological samples. The image can be enhanced by changing the emission properties of the fluorophores as we see with super-resolution light microscopy.[3–5] There are a number of ways to affect the emission properties that have been discovered including: (1) fluorescence quenching where molecules accept the energy from an excited fluorophore in the singlet state to prevent fluorescence through a nonradiative energy transfer,[6] (2) triplet quenchers that quench excited electrons in the slow emitting triplet state, (3) irregular fluctuation in fluorescence emission called fluorescence intermittency (or blinking), (4) photobleaching where the fluorophore interacts with a chemical damaging species, such as oxygen radicals, that damage the chemical structure and prevent further fluorescence and (5) in recent years, it has been noted that electrochemical potential can be used to modulate fluorescence emission either decreasing or enhancing the emission.[7–9] The ability to control the fluorescence emission through a potentially non-destructive method such as electrochemistry, provides the capability to remove the need for fluorescence and triplet quenching species, to illicit control over blinking, and to increase fluorescence emission to improve detection before photobleaching.

The range of fluorescent molecules that have been reported to undergo electrochemical induced fluorescence modulation have been as molecular fluorophores like rhodamine 101 (ref. 10) and Alexa Fluor 647,[11,12] and the proteins such as green fluorescent protein[5] and mCherry protein.[13] There has even been a reported case where the combination of a fluorescent molecule and the protein Azurin, a metalloprotein capable of undergoing redox controlled quenching, can result in dimming/

[a]School of Chemistry, The University of New South Wales, Sydney, New South Wales 2052, Australia. E-mail: justin.gooding@unsw.edu.au

[b]Australia Centre for NanoMedicine, The University of New South Wales, Sydney, New South Wales 2052, Australia

[c]Electron Microscope Unit, Mark Wainwright Analytical Centre, The University of New South Wales, Sydney, New South Wales 2052, Australia

† Electronic supplementary information (ESI) available. See DOI: https://doi.org/10.1039/d5sc01265a

© 2025 The Author(s). Published by the Royal Society of Chemistry

Open Access Article. Published on 15 April 2025. Downloaded on 3/21/2026 8:32:00 AM.
This article is licensed under a Creative Commons Attribution-NonCommercial 3.0 Unported Licence.

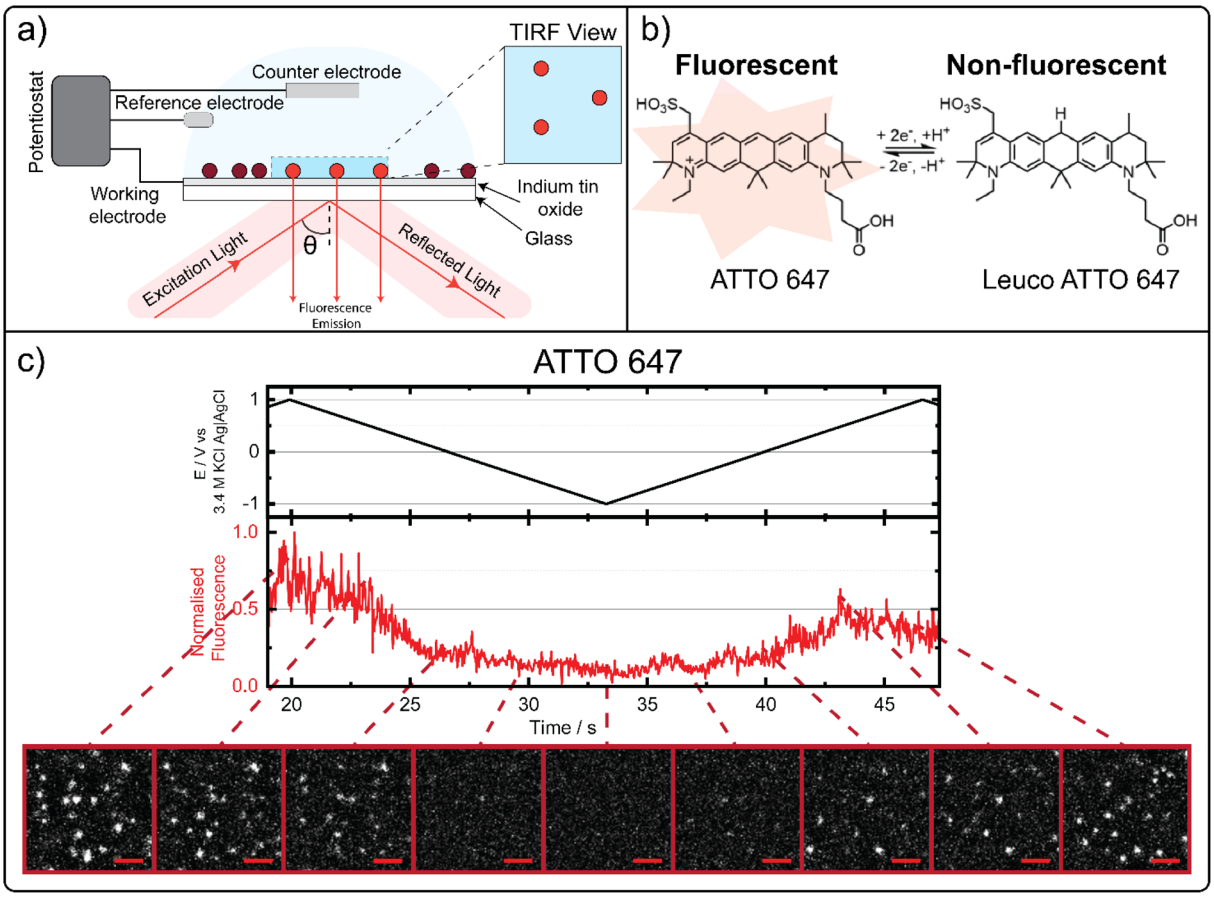

Fig. 1 (a) The sample is a glass coverslip coated with ITO. After adsorption of fluorophores to the ITO, the sample is connected to a potentiostat as the working electrode, a platinum wire is the counter electrode and a 3.4 M KCl Ag|AgCl reference electrode. (b) Using ATTO 647 as an example, a fluorophore is fluorescent in the oxidised state but is non fluorescent when the fluorophore is reduced into the leuco-state. (c) Electrochemical-induced fluorescence modulation of ATTO 647. ATTO 647 was adsorbed onto an ITO coated glass coverslip coated with poly-L-lysine and a cyclic voltammetry program of −1 V to 1 V at 150 mV s^{-1} was applied in 1X Dulbecco's phosphate buffered saline buffer (pH 7.4). Scale bars are 2 μm.

quenching of fluorescent molecules under oxidative potentials and the inverse for reduction potentials.[14] These examples demonstrate a diverse range of effective fluorescent species where electrochemistry is important in fluorescence microscopy. The coupling of electrochemistry with fluorescence has resulted in the development of electrochemical stochastic optical reconstruction microscopy (EC-STORM),[15] a method used to further increase the spatial resolution of super-resolution microscopy by controlling the blinking of fluorophores. Another example of utility is the work by Lu and co-workers where fluorescence modulation was used to detect the presence of redox active molecules.[7] The full capability of electrochemically controlling the fluorescence emission of fluorophores has yet to be utilised.

Herein, the role the chemical structure plays on the electrochemical-induced fluorescence modulation of fluorophores, and the effect of the buffer composition, are explored. The first aspect of chemical structure will cover different fluorescent structure variations, such as rhodamine, cyanine, and other fluorophore families. The second aspect is buffer composition where the oxygen level is changed and the addition of a triplet quencher is tested, as oxygen is reported to be responsible for photobleaching fluorophores,[16,17] and a triplet quencher removes triplet state transition to improve fluorescence. The experimental setup is displayed in Fig. 1a, where an indium tin oxide (ITO) coated glass coverslip is connected to a potentiostat and simultaneously viewed under a total internal reflection fluorescence (TIRF) microscope. Fluorescence modulation is a redox reaction where the oxidised state of a fluorophore is fluorescent, but the reduced state (radical and leuco-state) of the fluorophore is non-fluorescent as the $-N^{+}R_3$ group is reduced and a hydrogen ion is accepted, as displayed in Fig. 1b with ATTO 647 as the example. The fluorescence modulation is observed as a dimming and brightening of fluorophores, as shown in Fig. 1c.

Results and discussion

Structural analysis of fluorophore's

The first aspect to be explored is the susceptibility of different chemical structures to the electrochemical induced fluorescence modulation. The different chemical structures were categorized by the fluorescent core structures. The experiments

 © 2025 The Author(s). Published by the Royal Society of Chemistry

Open Access Article. Published on 15 April 2025. Downloaded on 3/21/2026 8:32:00 AM.
This article is licensed under a Creative Commons Attribution-NonCommercial 3.0 Unported Licence.

to determine a structures responsiveness were conducted in 1X Dulbecco's phosphate buffered saline (pH 7.4) and applied a cyclic voltammetry at −1 V to 0.3 V with a scan rate of 150 mV s^{-1}. Single molecule TIRF microscopy was employed to characterise the fluorescence at the single molecule level.

The fluorescent core structures tested were coumarin (ATTO 390), acridine (ATTO 495), rhodamine (ATTO 488, ATTO 565, and ATTO 590), xanthene (fluorescein), carbopyronine (ATTO 647), carborhodamine (ATTO 647N), cyanine (Alexa 647, CF 660C, and CF 680), and oxazine (ATTO 655). The fluorescence

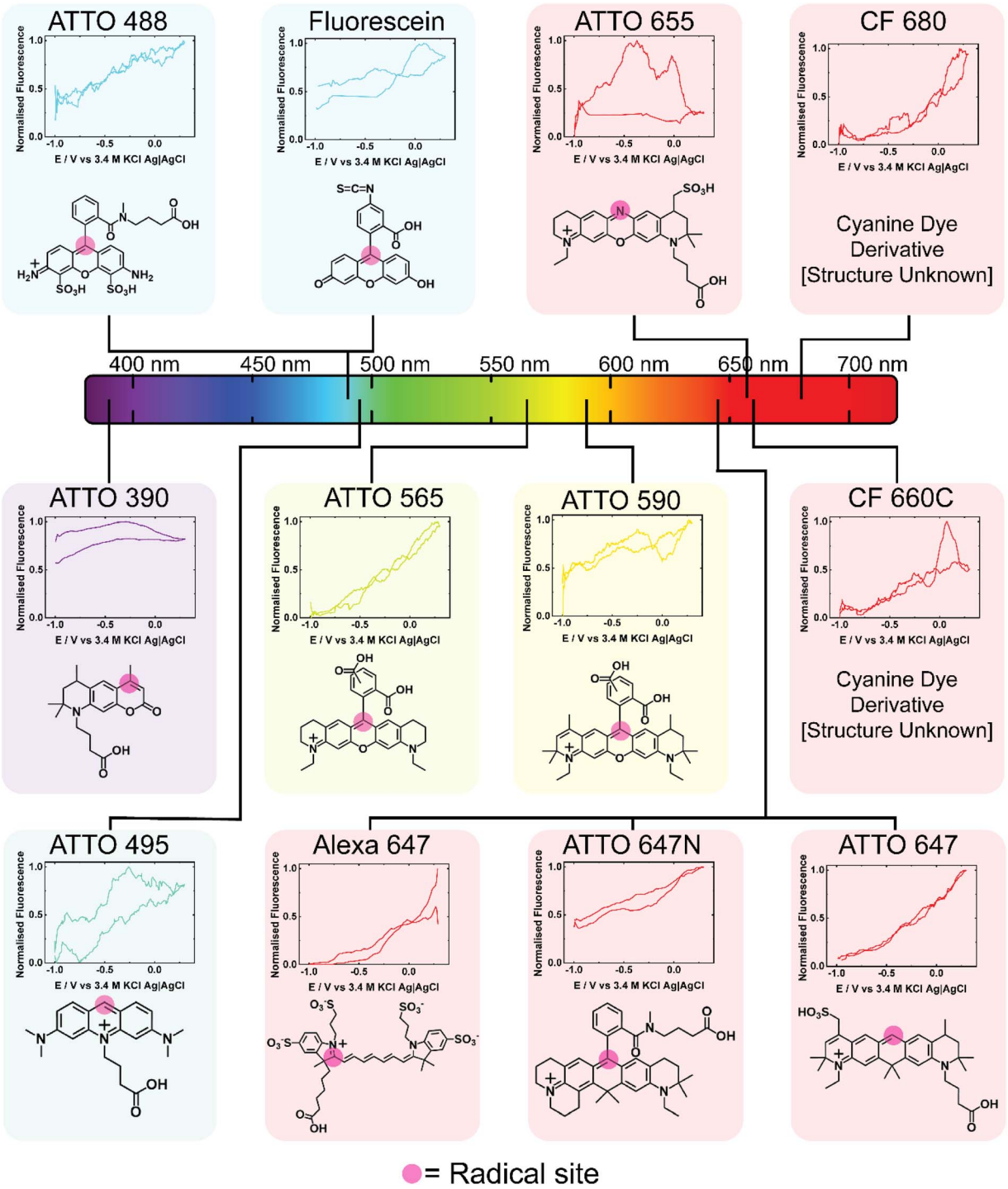

Fig. 2 The fluorophores ATTO 390 (coumarin), ATTO 488 (rhodamine), fluorescein isothiocyanate (xanthene), ATTO 495 (acridine), ATTO 565 (rhodamine), ATTO 590 (rhodamine), Alexa 647 (cyanine), ATTO 647 (carbopyronine), ATTO 647 (carborhodamine), ATTO 655 (oxazine), CF 660C (cyanine) and CF 680 (cyanine) are tested against a −1 V to 0.3 V cyclic voltammetry at 150 mV s^{-1} in 1X Dulbecco's phosphate buffered saline buffer (pH 7.4) and presented as optical cyclic voltammograms. Each optical CV was representative of at least 5 single molecule measurements over at least 6 cycles.

Open Access Article. Published on 15 April 2025. Downloaded on 3/21/2026 8:32:00 AM. This article is licensed under a Creative Commons Attribution-NonCommercial 3.0 Unported Licence.

output of a fluorophore was collected versus time, as shown in Fig. 1c. The time axis was converted to potential to directly correlate the change in fluorescence with potential, as presented in Fig. S1.† These plots are referred to as optical cyclic voltammograms.

Twelve optical cyclic voltammograms are shown in Fig. 2 for the twelve fluorophores investigated. The normalised fluorescence in Fig. 2 refers to how much the fluorescence emission of a single localised fluorophore changed with respect to the fluorophore's highest fluorescent emission at 1 V within the cycle between subsequent −1 V potentials. The normalised fluorescence was calculated by dividing the photon count at any potential within the complete cycle by the photon count at 1 V. The equation is as shown in eqn (1).

$$\text{Normalised fluorescence of cycle} = \frac{\text{photon count at potential}}{\text{photon count at 1V}} \quad (1)$$

All optical cyclic voltammograms in Fig. 2 are of a single molecule that is representative of other fluorophores with the same change in fluorescence response. The tracking of the single molecules was conducted over multiple cycles (upwards of 6) or until the fluorophore was photobleached and recurrence of a fluorophore at the same *x*- and *y*-coordinates between cycles confirmed that the fluorophores were adsorbed onto the surface. Of the twelve fluorophores, the fluorescence of eleven are observed to modulated with the potential. The fluorescence of ten fluorophores, all except ATTO 390 and ATTO 655, was modulated gradually with the changing potential. The gradual modulation of the fluorescence indicates that the electrochemical potential is driving the reaction between the oxidised fluorescent structure and the reduced non-fluorescent radical- and leuco-structure with the magnitude of the fluorescence reflecting the ratio of the two states at that potential.

ATTO 390 and ATTO 655 responded differently to the change in potential than the other ten fluorophores. ATTO 390 was the coumarin cored structure that was minimally responsive to potential as shown by the fluorescence increase at −0.3 V but primarily experienced photobleaching, as shown by the disconnect in normalised fluorescence at −1 V at the beginning and end of the cycle. ATTO 655 was the oxazine cored structure and became unlocalizable at the end of the anodic sweep. ATTO 655 remained unlocalizable for the cathodic sweep but was reactivated at the start of the subsequent anodic sweep. The unique response of ATTO 655 is speculated to be due to the non-fluorescent state being preferred over the fluorescent state under the potential range. The minimal electrochemical-induced fluorescence modulation pattern of ATTO 390, the unique modulation of ATTO 655, and the subtle difference in modulations of the remaining fluorophores, show the fluorescence modulation has a chemical structure dependency.

To complement the optical cyclic voltammogram's, the reaction mechanisms of three fluorophores are presented in Fig. 3. In Fig. 3, the reaction mechanism for oxazine, coumarin, and carbopyronine core structure are presented. The mechanism for the oxazine fluorophore was reported by van de Linde and co-workers,[18] and Lu and co-workers.[7] The mechanism for the coumarin fluorophore was reported by Wang and co-workers,[19] and Pasciak and co-workers.[20] The presented carbopyronine fluorophore mechanism is a proposed mechanism. The reported reactions entail the fluorescent structure being reduced electrochemically into a non-fluorescent semi-reduced radical form, followed by a transition to a non-fluorescent leuco state by the acceptance of a H^+ ion at the radical site, marked by a pink circle in Fig. 2.

Fig. 3 provides speculations as to why ATTO 390 and ATTO 655 as coumarin and oxazine dyes exhibited different response patterns. ATTO 390 will be discussed first. Comparison of chemical structures revealed that ATTO 390 lacks the electron withdrawing $-N^+R_3$ motif. Note the majority of the responsive fluorophores tested possess the electron withdrawing $-N^+R_3$ motif which suggests the $-N^+R_3$ motif is important for reduction and oxidation of the fluorophore within the tested potential range of −1 V to 0.3 V. The $-N^+R_3$ motif accepts an electron from the reorganisation of carbon double bonds upon reduction. There are two pieces of information worth noting. The first is that literature reported that coumarin structure reduces at potentials more negative than −1.3 V *vs.* Ag|AgCl.[19,20] However, the literature reported coumarin to undergo dimerization, as displayed in Fig. 3. That suggests that the coumarin fluorophore may not undergo the same reversible redox reaction as other fluorophores. The second is that ITO undergoes irreversible reduction to metallic indium at values greater than −1.2 V *vs.* Ag|AgCl at pH 7 (ref. 21) meaning that the coumarin reduction

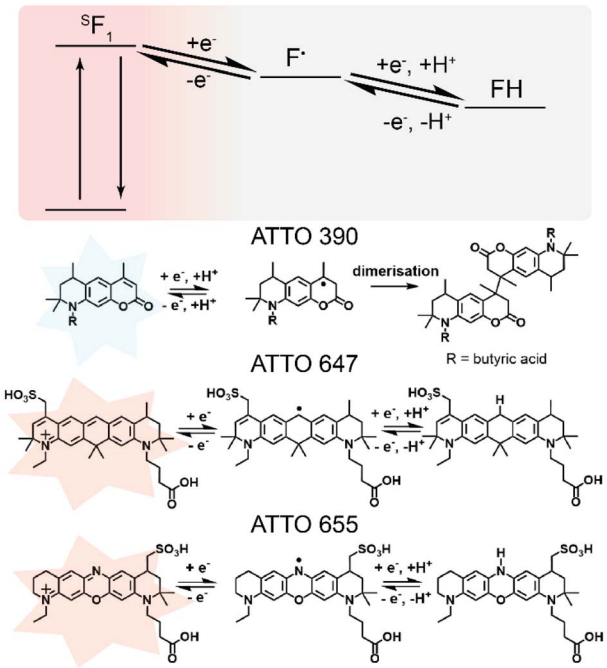

Fig. 3 The reversible reduction reactions of ATTO 390 (coumarin),[1,2] ATTO 647 (carbopyronine) (proposed), and ATTO 655 (oxazine).[3,4] The fluorophores enter a semi-reduced non fluorescent state and become a radical, the fluorophore is stabilised by accepting a H^+ ion under a reducing potential to enter the leuco-state. The reaction is reversed under a positive potential.

 © 2025 The Author(s). Published by the Royal Society of Chemistry

Open Access Article. Published on 15 April 2025. Downloaded on 3/21/2026 8:32:00 AM. This article is licensed under a Creative Commons Attribution-NonCommercial 3.0 Unported Licence.

potential is beyond the functional potential limit. Fluorescein isothiocyanate also lacks the electron withdrawing $-N^+R_3$ motif but remains responsive to potential changes as shown by going to and from a fluorescence ratio of 1.0 to 0.5 through the anodic and cathodic sweep. Fluorescein can readily transition between a non-fluorescent "closed" lactone configuration and a fluorescent "open" quinoid configuration. The lactone configuration is when the carboxylic acid group binds to the radical site.[22] The speculated reason for fluorescein's responsiveness is due to electrochemistry controlling the transition between the quinoid and lactone configuration. Furthermore, a phenazine derivative reported by Bezerra and co-workers, which lacked a $-N^+R_3$ motif, underwent electrochemical induced fluorescence modulation. The fluorescence modulation was achieved in the presence of a reducing agent of ascorbic acid, sodium dithionite, or a donor species such as triethylamine.[23] The modulation of fluorescein isothiocyanate and the phenazine derivative suggests that electrochemical induced fluorescence modulation can occur in the absence of a $-N^+R_3$ motif but a second reaction mechanism must be viable, or a reducing agent must be present. Based on the discussion, ATTO 390 may be capable of greater fluorescence modulation but the lack of a $-N^+R_3$ motif, a reducing agent, and a second reduction mechanism suggests that the potential range used in this paper could not transition ATTO 390 into a stable reduced non-fluorescent radical state.

Next, we will discuss ATTO 655. A comparison of the chemical structures revealed that ATTO 655 possesses a nitrogen at the radical site, the other ten responsive fluorophores possess a carbon. ATTO 655 and ATTO 647 possess a similar 5-ringed structure, but the radical site for ATTO 655 is nitrogen while for ATTO 647 is carbon, suggesting that elemental composition of the radical site affected the redox reaction displayed in Fig. 3. First, the lone pair of nitrogen are more stable in the imine configuration than the 2° amide configuration due to resonance stabilisation from the nitrogen double bonded to the carbon, however, the electrochemical potential can control the reduction to a 2° amide and stabilising the reduced configuration. Secondly, the electronegativity of an element is related to a radical's stability[24] and affects the bond dissociation energy required to remove a hydrogen. For example, the dissociation of a hydrogen from a carbon atom in cyclohexadiene is 310 kJ mol^{-1} while from a nitrogen atom in dimethylamine is 397 kJ mol^{-1}.[25] The difference in bond dissociation energy and radical stability are the suggested reasons for ATTO 655's different behaviour. That is the radical-ATTO 655 is more stable than radical-ATTO 647 and a greater oxidative potential is required remove the hydrogen from the leuco-ATTO 655 and restore fluorescence.

Furthermore, a review by Chicas-Baños and Frontana-Uribe reported that the potential and current required for dimerization of a molecule through the electrochemical generation of carbon and nitrogen centred radicals fluctuates.[26] The dimerization through the generation of a carbon-centred radical was reported to be achieved at 0.06 V *vs.* Ag|AgCl,[26] while for a nitrogen centred radical the potential was 1.2 V *vs.* Ag|AgCl.[26,27] However, these reported values are from two different reactions which utilized different chemicals. The review demonstrated that radical generation is different between two different chemicals and can explain the different response between other fluorophores. This speculation requires further testing of fluorophores that possess elements of different electronegativity at the radical site, elements such as boron, silicon, or phosphorous.

The above speculations regarding ATTO 390 and ATTO 655 unique modulation patterns suggest two things. The first is that the existence of the electron-withdrawing group $-N^+R_3$ motif facilitates the reduction within the operable range of ITO. The second is that structural variations, either elemental variations or different conjugation, changes the bond dissociation energy required to remove a hydrogen or radicalise a fluorophore and results in different modulation patterns.

Influence of buffer composition

The optical cyclic voltammogram's of Alexa 647, ATTO 647, and ATTO 647N from Fig. 2 were overlaid, as seen in Fig. S2,† and showed subtle differences between each fluorophore. Combining Alexa 647, ATTO 647, and ATTO 647N with ATTO 655 provided four fluorophore candidates with different fluorescent core structures within the same far-red fluorescent channel to investigate how different buffer additives may affect fluorescence modulation performance of different fluorescent structures.

Molecular 'triplet quenchers' increase the photon emission from fluorophores by depopulating/quenching their long-lived, slow-emitting triplet state. Oxygen is a fluorescence[28] and triplet quencher[29,30] but is simultaneously a photobleaching agent due to generation of organic-reactive singlet oxygens which irreversibly degrade fluorophores.[16,31,32] Another triplet quencher is (+/−)-6-hydroxy-2,5,7,8-tetramethylchromane-2-carboxylic acid (Trolox). The decrease of oxygen and addition of a triplet quencher may possess additional benefits for the electrochemical fluorescence modulation which will be explored within this section. The triplet quencher used in this section is Trolox, which was chosen due to the work by Fan and co-workers that demonstrated fluorescence modulation in the presence of Trolox.[11] To attain different oxygen levels in the buffer, the oxygen scavenger system known as 'gloxy' was used. Gloxy uses the enzyme's glucose oxidase and catalase in the presence of glucose to consume oxygen.[17] Buffers containing 'gloxy' would attain a lower molecular oxygen concentration and are referred to as 'low oxygen'. Buffers that do not contain an oxygen scavenger system would possess a higher molecular oxygen concentration and are referred to as 'high oxygen'. Fluorophores in the far-red fluorescent channel (Alexa 647, ATTO 647, ATTO 647N and ATTO 655) were used to assess how the buffer composition can affect fluorescence modulation. The optical CV of ATTO 655 in Fig. 2 indicates that the potential range of −1 V to 0.3 V was inadequate for ATTO 655 to undergo sufficient transition between the non-fluorescent and fluorescent state, prompting an increase potential range for the subsequent tests. For the following tests, a −1 V to 1 V cyclic voltammetry at a scan rate of 150 mV s^{-1} was applied to the four

Open Access Article. Published on 15 April 2025. Downloaded on 3/21/2026 8:32:00 AM.
This article is licensed under a Creative Commons Attribution-NonCommercial 3.0 Unported Licence.

fluorophores in the four different buffers at pH 7.4. The four buffers tested different oxygen and triplet quencher configurations. Buffer one was 1X Dulbecco's phosphate buffered saline (high oxygen and no Trolox). Buffer two was 1X Dulbecco's phosphate buffered saline and 2 mM Trolox (high oxygen and Trolox). Buffer three was 1X Dulbecco's phosphate buffered saline with gloxy (low oxygen and no Trolox). Buffer four was 1X Dulbecco's phosphate buffered saline with 2 mM Trolox and gloxy (low oxygen and Trolox). A combination of fluorescence emission against time, first displayed in Fig. 1c, and optical cyclic voltammograms, first displayed in Fig. 2, are used to attain quantitative comparison on the effect of the buffer composition. All experimental results are depicted in Fig. 4 and are determined from all localised fluorophores within the 51.2 μm × 51.2 μm field of view. The outputted fluorescence used for the results in Fig. 4 was normalised by the maximum fluorescent photon emission from all localised fluorophores.

To ascertain the impact of the buffer composition on a fluorophore's fluorescent properties, such as emission and stability, the mean photon emission rate at 1 V is used. The mean photon emission rate at 1 V for a fluorophore is calculated in two steps. The first step is to divide the total fluorescent photon emission of all localised fluorophores by the number of localised fluorophores at 1 V for each cycle to attain the mean photon emission at 1 V. The second step is to average the mean photon emission at 1 V attained in subsequent cycles and divide by the exposure time to attain the mean photon emission rate at 1 V and the corresponding standard deviation between cycles. An increase in the photon emission rate value means an improvement in detection and the contrast between reducing and oxidising potentials. A low standard deviation suggests greater stability and longevity of fluorophore between multiple cycles.

In Fig. 4a, the mean photon rate at 1 V is graphed for each fluorophore in each buffer. The photon emission rate for Alexa 647 in the high oxygen buffer with no Trolox, the low oxygen buffer with no Trolox, the high oxygen buffer with Trolox, and the low oxygen buffer with Trolox are 5.1 ± 2.0 photons m s^{-1}, 6.6 ± 2.0 photons m s^{-1}, 5.2 ± 0.14 photons m s^{-1}, and 12 ± 0.58 photons m s^{-1}, respectively. In the buffer with low oxygen and Trolox, Alexa 647 attained the highest photon emission rate, and the second smallest standard deviation, as shown in Fig. 4a. The larger photon emission rate affirmed that Alexa 647 has improved fluorescent properties, and the smaller standard deviation affirmed that Alexa 647 was more stable and was undergoing less photobleaching. The photon emission rate for ATTO 647 in the high oxygen and no Trolox, high oxygen and Trolox, low oxygen and no Trolox, and low oxygen and Trolox buffers are 7.3 ± 0.77 photons m s^{-1}, 5.5 ± 0.60 photons m s^{-1}, 8.4 ± 0.84 photons m s^{-1}, and 8.0 ± 1.9 photons m s^{-1}, respectively. These results were determined to not be statistically significant, as shown in Fig. 4a, which affirmed that ATTO 647 did not attain an improved fluorescent emission or stability in the tested buffer compositions. The photon emission rate for ATTO 647N in the high oxygen and no Trolox, high oxygen and Trolox, low oxygen and no Trolox, and low oxygen and Trolox buffers are 7.9 ± 4.8 photons m s^{-1}, 7.1 ± 2.0 photons m s^{-1}, 9.6 ± 4.0 photons m s^{-1}, and 7.4 ± 2.9 photons m s^{-1}, respectively.

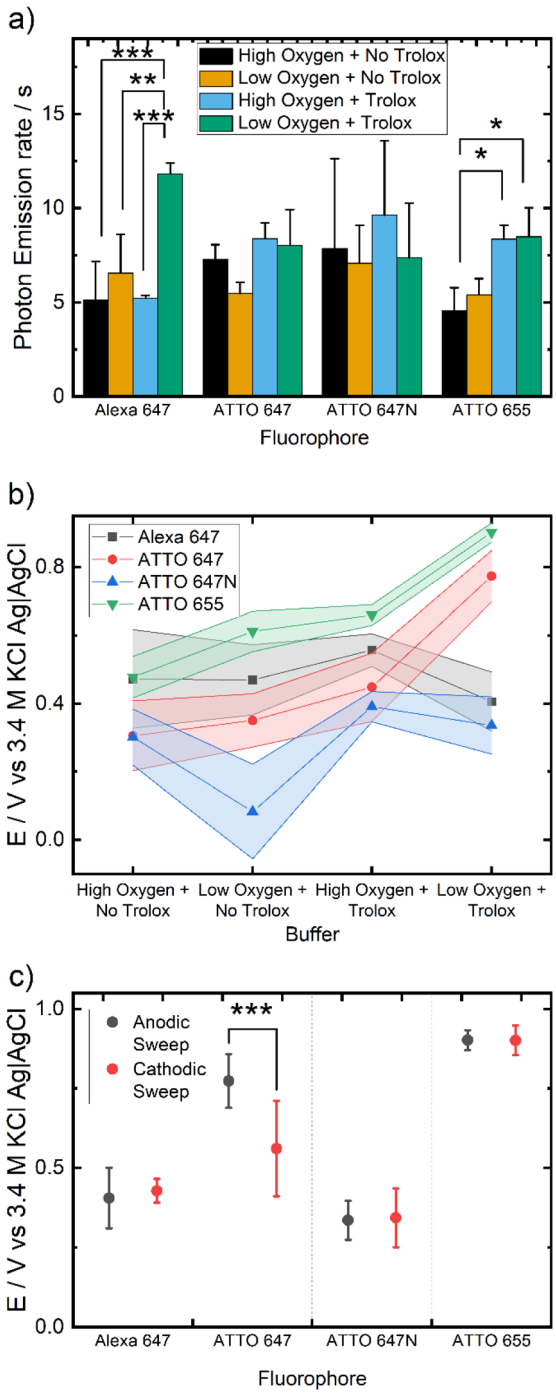

Fig. 4 (a) The mean photon emission at 1 V for Alexa 647, ATTO 647, ATTO 647N, and ATTO 655 in the four buffer configurations of differing oxygen level and Trolox presence. (b) The midpoint potential from the anodic sweep of the −1 V to 1 V cyclic voltammetry at 150 mV s^{-1} for Alexa 647, ATTO 647, ATTO 647N, and ATTO 655 in four buffer configurations, buffer one is high oxygen with no Trolox, buffer two is low oxygen with no Trolox, buffer three is high oxygen with Trolox, and buffer four is low with Trolox. The results are determined from all localised fluorophores with the variance shown by the shaded regions around each line. (c) Comparison of the midpoint potentials of the anodic (black points) and cathodic (red points) sweep for each fluorophore in the buffer configuration of low oxygen and containing Trolox. *$p \leq 0.05$, **$p \leq 0.01$, ***$p \leq 0.001$.

 © 2025 The Author(s). Published by the Royal Society of Chemistry

Open Access Article. Published on 15 April 2025. Downloaded on 3/21/2026 8:32:00 AM. This article is licensed under a Creative Commons Attribution-NonCommercial 3.0 Unported Licence.

These results are also not statistically significant, as shown in Fig. 4a, which affirmed that ATTO 647N did not attain an improved fluorescent emission. The size of the standard deviation suggests that ATTO 647N was suffering from photobleaching. The photon emission rate for ATTO 655 in the high oxygen and no Trolox, high oxygen and Trolox, low oxygen and no Trolox, and low oxygen and Trolox buffers are 4.6 ± 1.2 photons m s^{-1}, 5.4 ± 0.86 photons m s^{-1}, 8.3 ± 0.76 photons m s^{-1}, 8.5 ± 1.5 photons m s^{-1}, respectively. The improvement in photon emissions for the buffers that contain Trolox is statistically significant from buffers without Trolox. The results collected confirm that ATTO 647N and ATTO 647 are not drastically affected by the buffer composition, while Alexa 647 performed better in the low oxygen buffer with Trolox and ATTO 655 performed better in a buffer with Trolox present. [discuss mechanism].

The midpoint potential is when the ratio between the fluorescent and non-fluorescent state is halfway between the normalized maximum and minimum ratio achieved between the observed potential range, which is −1 V to 1 V for this paper. The midpoint point potential was used to indicate how buffer composition affected the electrochemical induced fluorescence modulation behaviour. To measure the midpoint potential, the sum of the fluorescent photon emission from all localised fluorophores was plotted into an optical cyclic voltammogram. The optical cyclic voltammogram was smoothed using OriginLabs 'Adjacent Averaging' set to 25, normalized, and then the optical cyclic voltammogram was separated into anodic sweeps and cathodic sweeps. For each cathodic and anodic sweeps, the midpoint potential was determined by using OriginLabs fitting program to fit a Boltzmann sigmoidal to the data, as shown in Fig. S3.† The Boltzmann sigmoidal was used to determine when the photon emission sum of all fluorophores reached halfway between the maximum and minimum between −1 V and 1 V. For the anodic and cathodic sweeps, four midpoint potentials from the sweeps from four cycles were averaged and the standard deviation represented the consistency the fluorophores attained the averaged midpoint potential between the cycles. The cathodic sweep increases the occurrence of the non-fluorescent structure and relates to the potential required to reduce the fluorophore structure to the non-fluorescent leuco structure. The anodic sweep increases the occurrence of the fluorescent structure and relates to the potential required to remove the hydrogen from the radical site through oxidation and restore the conjugation in the fluorescent structure.

The anodic midpoint potential results are presented in Fig. 4b, the cathodic midpoint potentials are in Fig. S4.† The anodic midpoint potentials of ATTO 655 in the high oxygen with no Trolox, low oxygen with no Trolox, high oxygen with Trolox, and low oxygen with Trolox buffer compositions are 0.48 ± 0.061 V, 0.61 ± 0.059 V, 0.66 ± 0.030 V, and 0.90 ± 0.028 V, respectively. The positive shift in the anodic potential indicates the ratio between the fluorescence and non-fluorescent state shifted between the different buffers, either stabilising the radical-ATTO 655 and/or increased the formation of the leuco-ATTO 655. The anodic midpoint potentials of Alexa 647 in the high oxygen with no Trolox, low oxygen with no Trolox, high oxygen with Trolox, and low oxygen with Trolox buffer compositions are 0.47 ± 0.14 V, 0.47 ± 0.10 V, 0.56 ± 0.048 V, and 0.41 ± 0.087 V, respectively. The anodic midpoint potentials do not change significantly, indicating that the buffer composition did not greatly affect the redox reaction of Alexa 647. The anodic midpoint potentials of ATTO 647 in the high oxygen with no Trolox, low oxygen with no Trolox, high oxygen with Trolox, and low oxygen with Trolox buffer compositions are 0.31 ± 0.10 V, 0.35 ± 0.079 V, 0.45 ± 0.10 V, and 0.77 ± 0.076 V, respectively. The shift in the anodic midpoint potential in the buffer of low oxygen with Trolox for ATTO 647 suggested that the low-oxygen and Trolox stabilised the radical- and leuco-ATTO 647. The buffer affected the fluorescence modulation of ATTO 647 by shifting the ratio between fluorescent and non-fluorescent structure. The anodic midpoint potential of ATTO 647N in the high oxygen with no Trolox, low oxygen with no Trolox, high oxygen with Trolox, and low oxygen with Trolox buffer compositions are 0.30 ± 0.083 V, 0.083 ± 0.14 V, 0.39 ± 0.044 V, and 0.34 ± 0.085 V, respectively. The lack of variation in the anodic potential showed that ATTO 647N was not affected by the addition of Trolox. However, the low oxygen buffer decreased the stability of the radical- and leuco-ATTO 647N and affected the fluorescence modulation of ATTO 647N.

A notable observation is that in the two buffer compositions of low oxygen with and without Trolox, the different anodic midpoint potentials for three fluorophores are statistically significant, as shown in Fig. S5.† In the buffer of low oxygen with no Trolox, the anodic midpoint potentials of ATTO 655 and ATTO 647N are statistically significant from each other and from the anodic midpoint potential of Alexa 647 and ATTO 647. In the buffer of low oxygen with Trolox, the different anodic midpoint potentials of ATTO 655 and ATTO 647 are statistically significant from each other and from the anodic midpoint potentials of Alexa 647 and ATTO 647N. This observation of different anodic midpoint potentials affirms that the radical and leuco structure of the different fluorophores have different stabilities to each other and in different buffers, which confirmed that the chemical and the buffer affected the observed fluorescence modulation.

The results have shown that the electrochemical induced fluorescence mechanism is affected by the oxygen concentration and the presence of the triplet quencher Trolox. Oxygen is a fluorescence and triplet quencher and a photobleaching agent, the removal of oxygen influences the mechanism in three ways. The first is to increase fluorescence from fluorophores through removal of fluorescence quenching. The second is to prevent photobleaching of fluorophores from oxygen radicals to increase fluorophore longevity. The third is that the removal of oxygen stabilises the non-fluorescent radical or leuco-state for ATTO 655 and ATTO 647, increasing the prevalence of the non-fluorescent states. With regards to the addition of Trolox, the suggested mechanism is that the fluorophores triplet state is in competition with the electrochemically reduced non-fluorescent states and the quenching of the triplet states with increase the prevalence and stability of the electrochemically reduced non-fluorescent states.

Open Access Article. Published on 15 April 2025. Downloaded on 3/21/2026 8:32:00 AM. This article is licensed under a Creative Commons Attribution-NonCommercial 3.0 Unported Licence.

Closer examination of the optical cyclic voltammograms conducted in the buffer that contained low oxygen and Trolox, the fluorescence modulation in the anodic sweep and cathodic sweep were comparable for both Alexa 647 and ATTO 647N, as seen in Fig. S6a and c.† For ATTO 655 and ATTO 647, there is an observed different point at which the normalised fluorescence diverged away from the *x*-axis between the anodic and cathodic sweeps which indicated the transition between the fluorescence and non-fluorescent states is affected by the sweep polarity, as seen in Fig. S6b and d.† In particular, the anodic sweep the nonfluorescent reduced ATTO 655 became fluorescent was at ≈ 0.4 V but in the cathodic sweep the normalised fluorescence of ATTO 655 reached ≈ 0 at ≈ −0.2 V, shown in Fig. S6.† The hysteresis between the cathodic and anodic sweep of ATTO 655 suggests that the leuco-state became stable and required a greater oxidative potential to restore the fluorescent structure. Comparison of the cathodic and anodic midpoint potentials for Alexa 647, ATTO 647, ATTO 647N, and ATTO 655 are plotted in Fig. 4c and was used to confirm the separation between the cathodic and anodic sweeps. The anodic and cathodic midpoint potentials for Alexa 647 was 0.41 ± 0.087 V and 0.43 ± 0.034 V, respectively, for ATTO 647N was 0.34 ± 0.084 V and 0.34 ± 0.085 V, respectively, and for ATTO 655 was 0.90 ± 0.028 V and 0.90 V ± 0.042 V, respectively. The separation between the anodic and cathodic midpoint potentials for Alexa 647, ATTO 647N, and ATTO 655 were not statistically significant. This suggests that the ratio between the fluorescent and non-fluorescent rates are directly correlated to the potential. However, ATTO 655 possessed a different point at which the normalised fluorescence diverged from the *x*-axis between the anodic and cathodic sweeps. For ATTO 655, the intensity approaches 0 at around −1 V in the cathodic sweep and remains non-fluorescent until 0.66 ± 0.012 V in the anodic sweep. This suggests that leuco-ATTO 655 is stable. The similar cathodic and anodic midpoint potential indicates that once the long-lived leuco-state is reversed, the ratio between the fluorescent state and the non-fluorescent radical state became proportional to the potential. ATTO 647 attained anodic and cathodic midpoint potentials of 0.77 ± 0.076 V and 0.56 ± 0.13 V, respectively, and the difference was determined to be statistically significant. This result affirmed that for ATTO 647 the ratio between the fluorescent and non-fluorescent state is dependent on the sweep polarity. As the potential to reduce ATTO 647 to a long-lived non-fluorescent leuco-state is different than the potential required to oxidise the leuco-ATTO 647 to restore fluorescence. The difference between the midpoint potentials from the anodic and cathodic sweep for ATTO 647 provided evidence that the leuco-ATTO 647 are more stable than the leuco-Alexa 647 and leuco-ATTO 647N. The different stability is speculated to be due to different dissociation energy required to remove the hydrogen that was bound to the radical site due to different chemical structure. More investigation into other fluorophores and buffer compositions can provide insight into the mechanism. All results collected confirm that the electrochemical induced fluorescence modulation is subjected to change based on the fluorophores chemical structure and buffer composition.

A final remark, the anodic midpoint potential confirmed that the chemical structure and buffer composition affected the fluorescence modulation but can be supplemented with the mean photon emission at 1 V. For example, in the low oxygen buffer with Trolox, Alexa 647 and ATTO 647N have similar anodic midpoint potentials which suggests the two structures are modulated the same. However, Alexa 647 achieved a greater mean photon emission at 1 V than ATTO 647N. Which suggests that Alexa 647 underwent a greater total change of fluorescence than ATTO 647N and that the ratio between Alexa 647 and leuco-Alexa647 was more responsive to the changing potential.

Conclusions

The results have shown that the structure and the buffer composition affected the fluorescence modulation of a fluorophore. Any structural variations will contribute to fluorescence modulation of a fluorophore, that can be used as a 'fingerprint'. The structural variations influence the stability of the radical state, and the energy required to reduce the fluorophore structure, while change the bond dissociation energy required to separate the hydrogen from the leuco-fluorophore. The greater the structural difference between two fluorophores, such as different fluorescent core structure, the more identifiable the resultant pattern of modulated fluorescence will be with respect to the two fluorophores. The investigation into the structure has provided two key speculations. The first is that the presence of the electron withdrawing motif $-N^{+}R_3$ facilitates fluorescence modulation within the operable range of ITO, as shown with ATTO 390 minimal observed response. The second is that the elemental configuration of the radical site can greatly affect the resultant pattern of modulated fluorescence. Elemental configuration will influence the radical stability and the bond dissociation energies of the hydrogen, as shown by ATTO 655. Further experimentation on more fluorescent structures is required to confirm the mentioned speculations, such as testing different elements at the radical site and different electron withdrawing groups.

The buffer compositions can affect either the fluorescent properties and/or the electrochemical induced fluorescence modulation. The buffer containing low oxygen and Trolox presented two unique changes to the electrochemical induced fluorescence modulation. The first is that the photon emission rate at 1 V for Alexa 647 was greater than in the other compositions. The increased photon emission resulted in a greater change in fluorescence emission and was caused by destabilising the radical- and leuco-state to make the fluorescent state more prevalent. The second is that for ATTO 647 and ATTO 655, these two fluorophores were shown to enter a stable non-fluorescent leuco-state which required the correct oxidative potential to restore fluorescence. The non-fluorescent states became stabilised as determined by the positive shift in anodic midpoint potentials with the different buffers. Further experimentation into different buffer compositions can provide greater control over the electrochemical fluorescence modulation.

 © 2025 The Author(s). Published by the Royal Society of Chemistry

Open Access Article. Published on 15 April 2025. Downloaded on 3/21/2026 8:32:00 AM. This article is licensed under a Creative Commons Attribution-NonCommercial 3.0 Unported Licence.

Methods

Materials and chemicals

Fluorophores ATTO 390, ATTO 488, ATTO 495, ATTO 565, ATTO 590, ATTO 647, ATTO 647, ATTO 655 (all from ATTO-TEC), Alexa 647 (ThermoFisher), CF 660C (Sigma-Aldrich) and CF 680 (Sigma-Aldrich) were purchased with NHS-ester functional group and used as provided. Fluorescein isothiocyanate (Sigma-Aldrich) was purchased and used as provided. 1X Dulbecco's phosphate buffered saline buffer without magnesium and calcium was purchased from Thermo Fisher and prior to usage, solution was filtered using a 0.22 μm polyethersulfane membrane filter. D-(+)-Glucose (Sigma Aldrich, ≥99.5%), glucose oxidase from *Aspergillus niger* type X-S (Sigma-Aldrich), catalase from bovine liver (Sigma-Aldrich), (±)-6-hydroxy-2,5,7,8-tetramethylchromane-2-carboxylic acid (Sigma-Aldrich, 97%), 0.1% w/v poly-L-lysine solution (Sigma-Aldrich) and anhydrous dimethyl sulfoxide (DMSO) (Sigma-Aldrich, ≥ 99%) were used as received. 22 × 22 mm ITO coated glass coverslips with a resistivity of 8–12 Ω per square acquired from SPI Supplies.

Sample preparation

ITO coated glass coverslips were plasma cleaned using a Harrick Plasma PDC-002 at 600 mtorr pressure set on high power. The cleaned ITO coated glass coverslips were exposed to 100 μL of a poly-L-lysine dilution, made by a 1 : 1 dilution of 0.1 w/v% poly-L-lysine solution with 1X Dulbecco's phosphate buffered saline buffer, for 30 min to coat the ITO coated glass coverslip with poly-L-lysine. A 1 mg mL^{-1} fluorophore solution in DMSO of all fluorophores was prepared. A 10^{-4} mg mL^{-1} dilution of each tested fluorophore is made by diluting the stock 1 mg mL^{-1} fluorophore solution with 1X Dulbecco's PBS buffer. Prior to imaging, the poly-L-lysine coated ITO coated glass coverslips were exposed to 100 μL of the 10^{-4} mg mL^{-1} fluorophore dilution for 5 min to allow for fluorophore adsorption onto the surface, followed by being lightly rinsed with 1X Dulbecco's phosphate buffered saline buffer to remove non-adsorbed fluorophores. The sample with the fluorophores adsorbed onto the poly-L-lysine coated ITO coated glass coverslip were loaded into a custom-made electrochemical Chamlide fluidic cell made by LCI (Live Cell Instrument).

Buffer preparation

Four buffers are prepared and used for experimentation throughout this paper. Buffer one was 1X Dulbecco's phosphate buffered saline (without magnesium and calcium) at pH 7.4. Buffer two was 1X Dulbecco's phosphate buffered saline (without magnesium and calcium) and 2 mM Trolox at pH 7.4. Buffer three was 1X Dulbecco's phosphate buffered saline (without magnesium and calcium), 10% w/v glucose, 0.5 mg mL^{-1} glucose oxidase, 40 μg mL^{-1} catalase at pH 7.4. Buffer four was 1X Dulbecco's phosphate buffered saline (without magnesium and calcium), 10% w/v glucose, 0.5 mg mL^{-1} glucose oxidase, 40 μg mL^{-1} catalase, and 2 mM Trolox at pH 7.4.

Table 1 The excitation wavelength and power density of the lasers used to excite the fluorophores

Fluorophore	Laser $\lambda_{excitation}$/nm	Laser power density/kW cm^{-2}
ATTO 390	405	0.12
ATTO 488	488	0.97
ATTO 495	488	0.10
ATTO 565	561	1.9
ATTO 590	561	1.9
Alexa 647	642	1.5
ATTO 647	642	1.5
ATTO 647N	642	1.5
ATTO 655	642	1.5
CF 660C	642	2.2
CF 680	642	2.2

Fluorescence microscopy, single molecule imaging and electrochemical induced photoswitching

The microscope used was a Zeiss Elyra PALM/SIM (Zeiss Axio Observer.Z1) microscope with a single molecule localisation microscope camera, EM CCD with Carl Zeiss™ Immersol™ Immersion 518F 25 °C 100× oil, with laser angle ≈ 66° to undergo total internal reflection and a α Plan-Apochromat 100×/1.46 Oil DIC M27 Elyra objective lens. The microscope possessed four fluorescent channels. The channels are referred to throughout this paper as the blue, green, red, and far-red channel, the lasers used for the channels are 405 nm, 488 nm, 561 nm and 642 nm, respectively and the filters are BP 420–488 + LP 750, LP 495–575 + LP 750, BP 570–650 + LP 750 and LP 655, respectively. The excitation laser and laser power density for each fluorophore is listed in Table 1.

The electrochemical techniques were controlled by a Bio-Logic SP-200 potentiostat. The working electrode was the functionalised ITO coated glass coverslip surface connected using a spring-loaded gold coated pin, the counter electrode was a platinum wire, and the reference electrode was a leak-free 3.4 M KCl Ag|AgCl reference electrode purchased from Innovative Instruments. The electrochemical technique performed was cyclic voltammetry. The cyclic voltammetry parameters were −1 V to 0.3 V and −1 V to 1 V, both were at a scan rate of 150 or 300 mV s^{-1} (scan rate was adjusted based on the photobleaching of the individual fluorophores) and were recorded for approximately 2–3 minutes. Unilluminated areas of the sample were used for subsequent experiments.

Data analysis

Data analysis was accomplished with a two-step procedure. The first step used the Zeiss ZEN (Black Edition)[33] software to localise the single molecule fluorescent fluorophores from the recorded video and output the localisation events into a localisation data table. The Zeiss ZEN (Black Edition)[33] software localised the fluorophores using a peak intensity to noise value of 4–6 (dependent on the fluorophore and sample), a peak mask size of 9, and was set to ignore overlap. Zeiss ZEN (Black Edition)[33] software removed noise by accepting localisations with a point spread function between to 110–500 nm,

Open Access Article. Published on 15 April 2025. Downloaded on 3/21/2026 8:32:00 AM. This article is licensed under a Creative Commons Attribution-NonCommercial 3.0 Unported Licence.

localisation precision between to 1–110 nm, and chi square between to 0–0.8. The second step used a Matlab[34] script that converted the localisation data table into a second table consisting of the 'frame number', 'time/s', '*E*/*V vs.* 3.4 M KCl Ag|AgCl', 'mean photon emission', 'sum photon emission' and 'localised spots'. The second table's results were graphed using the OriginLab[35] graphing software.

Data availability

The data supporting this article have been included as part of the ESI.†

Author contributions

Daniel Hagness: experimentation, conceptualization, investigation, visualization, writing–original draft, writing–review & editing. Ying Yang: writing–original draft, writing–review & editing. Yuanqing Ma: experimentation, supervision. Sumaya Ishtiaq: experimentation. Sanjun Fan: experimentation. Richard D. Tilley: supervision, writing–review & editing. J. Justin Gooding: conceptualisation, supervision, writing–review & editing, funding acquisition, project administration.

Conflicts of interest

The authors declare that they have no known competing financial interests or personal relationships that could have appeared to influence the work reported in this paper.

Acknowledgements

Daniel E. Hagness acknowledges support from the Australian Government Research Training Program (RTP) Scholarship. J. Justin Gooding acknowledges the Australian Research Council Discovery Grant Program (DP220103024) and a National Health and Medical Research Council Investigator Grant (GNT1196648). Richard D. Tilley acknowledges funding from the Australian Research Council Discovery Grants (DP190102659 and DP200100143).

Notes and references

1 O. Heimstädt and D. fluoreszenzmikroskop, *Z. Wiss. Mikrosk. Mikrosk. Tech.*, 1911, **28**, 330–337.
2 A. J. Wollman, R. Nudd, E. G. Hedlund and M. C. Leake, From Animaculum to single molecules: 300 years of the light microscope, *Open Biol.*, 2015, **5**, 150019.
3 M. J. Rust, M. Bates and X. Zhuang, Sub-diffraction-limit imaging by stochastic optical reconstruction microscopy (STORM), *Nat. Methods*, 2006, **3**, 793–796.
4 M. Heilemann, S. Van De Linde, M. Schüttpelz, R. Kasper, B. Seefeldt, A. Mukherjee, P. Tinnefeld and M. Sauer, Subdiffraction-resolution fluorescence imaging with conventional fluorescent probes, *Angew. Chem., Int. Ed.*, 2008, **47**, 6172–6176.
5 T. Dertinger, R. Colyer, G. Iyer, S. Weiss and J. Enderlein, *Fast, Background-free, 3D Super-Resolution Optical Fluctuation Imaging (SOFI)*, Proceedings of the National Academy of Sciences, 2009, 106, pp. 22287–22312.
6 J. Ashley and P. Manikova, in *Fundamentals of Sensor Technology*, ed. A. Barhoum and Z. Altintas, Woodhead Publishing, 2023, pp. 147–161, DOI: **10.1016/B978-0-323-88431-0.00022-3**.
7 J. Lu and M. D. Lew, Single-molecule electrochemical imaging resolves the midpoint potentials of individual fluorophores on nanoporous antimony-doped tin oxide, *Chem. Sci.*, 2024, **15**(6), 2037–2046.
8 Y. Yang, S. Fan, J. A. Webb, Y. Ma, J. Goyette, X. Chen, K. Gaus, R. D. Tilley and J. J. Gooding, Electrochemical fluorescence switching of enhanced green fluorescent protein, *Biosens. Bioelectron.*, 2023, 115467.
9 K. Nakamura, K. Kanazawa and N. Kobayashi, Electrochemical photoluminescence modulation of functional materials and their electrochemical devices, *J. Photochem. Photobiol., C*, 2022, **50**, 100486.
10 M. Čížková, L. Cattiaux, J.-M. Mallet, E. Labbé and O. Buriez, Electrochemical switching fluorescence emission in rhodamine derivatives, *Electrochim. Acta*, 2018, **260**, 589–597.
11 S. Fan, J. E. A. Webb, Y. Yang, D. J. Nieves, V. R. Gonçales, J. Tran, G. Hilzenrat, M. Kahram, R. D. Tilley, K. Gaus and J. J. Gooding, Observing the Reversible Single Molecule Electrochemistry of Alexa Fluor 647 Dyes by Total Internal Reflection Fluorescence Microscopy, *Angew. Chem., Int. Ed.*, 2019, **58**, 14495–14498.
12 Y. Yang, Y. Ma and J. J. Gooding, The electrochemical modulation of single molecule fluorescence, *Faraday Discuss.*, 2025, **257**, 333–343.
13 Y. Fan, Z. Chen and H.-w. Ai, Monitoring redox dynamics in living cells with a redox-sensitive red fluorescent protein, *Anal. Chem.*, 2015, **87**, 2802–2810.
14 L. Jeuken, M. Orrit and G. Canters, Single-molecule fluorescence in redox chemistry, *Curr. Opin. Electrochem.*, 2022, 101196.
15 Y. Yang, Y. Ma, J. F. Berengut, L. K. Lee, R. D. Tilley, K. Gaus and J. J. Gooding, Electrochemically controlled blinking of fluorophores for quantitative STORM imaging, *Nat. Photonics*, 2024, **18**, 713–720.
16 Q. Zheng, S. Jockusch, Z. Zhou and S. C. Blanchard, The contribution of reactive oxygen species to the photobleaching of organic fluorophores, *Photochem. Photobiol.*, 2014, **90**, 448–454.
17 C. E. Aitken, R. A. Marshall and J. D. Puglisi, An oxygen scavenging system for improvement of dye stability in single-molecule fluorescence experiments, *Biophys. J.*, 2008, **94**, 1826–1835.
18 S. Van De Linde and M. Sauer, How to switch a fluorophore: from undesired blinking to controlled photoswitching, *Chem. Soc. Rev.*, 2014, **43**, 1076–1087.
19 L.-H. Wang and H.-H. Liu, Electrochemical reduction of coumarins at a film-modified electrode and determination

 © 2025 The Author(s). Published by the Royal Society of Chemistry

Open Access Article. Published on 15 April 2025. Downloaded on 3/21/2026 8:32:00 AM.
This article is licensed under a Creative Commons Attribution-NonCommercial 3.0 Unported Licence.

of their levels in essential oils and traditional Chinese herbal medicines, *Molecules*, 2009, **14**, 3538–3550.

20 E. M. Pasciak, J. T. Rittichier, C.-H. Chen, M. S. Mubarak, M. S. VanNieuwenhze and D. G. Peters, Electroreductive dimerization of coumarin and coumarin analogues at carbon cathodes, *J. Org. Chem.*, 2015, **80**, 274–280.

21 L. Liu, S. Yellinek, I. Valdinger, A. Donval and D. Mandler, Important implications of the electrochemical reduction of ITO, *Electrochim. Acta*, 2015, **176**, 1374–1381.

22 K. Kanazawa, K. Nakamura and N. Kobayashi, High-contrast electroswitching of emission and coloration based on single-molecular fluoran derivatives, *J. Phys. Chem. A*, 2014, **118**, 6026–6033.

23 L. F. Bezerra, T. F. Paulo, I. M. de Carvalho, F. S. G. Júnior, L. G. Lopes and I. C. Diógenes, Redox-responsive fluorescence emission output of a synthetic phenazine derivative, *Dyes Pigm.*, 2023, **216**, 111375.

24 M. Lazár, *Free Radicals In Chemistry And Biology*, CRC press, 1989.

25 J. A. Dean, *Lange's Handbook of Chemistry*, 15th edn, 1999, pp. 4–46.

26 D. F. Chicas-Baños and B. A. Frontana-Uribe, Electrochemical Generation and Use in Organic Synthesis of C-, O-, and N-Centered Radicals, *Chem. Rec.*, 2021, **21**, 2538–2573.

27 B. R. Rosen, E. W. Werner, A. G. O'Brien and P. S. Baran, Total synthesis of dixiamycin B by electrochemical oxidation, *J. Am. Chem. Soc.*, 2014, **136**, 5571–5574.

28 J. R. Lakowicz and G. Weber, Quenching of fluorescence by oxygen. Probe for structural fluctuations in macromolecules, *Biochemistry*, 1973, **12**, 4161–4170.

29 C. Grewer and H.-D. Brauer, Mechanism of the triplet-state quenching by molecular oxygen in solution, *J. Phys. Chem.*, 1994, **98**, 4230–4235.

30 J. Strömqvist, A. Chmyrov, S. Johansson, A. Andersson, L. Mäler and J. Widengren, Quenching of triplet state fluorophores for studying diffusion-mediated reactions in lipid membranes, *Biophys. J.*, 2010, **99**, 3821–3830.

31 J. Xu, S. Fan, L. Xu, A. Maruyama, M. Fujitsuka and K. Kawai, Control of Triplet Blinking Using Cyclooctatetraene to Access the Dynamics of Biomolecules at the Single-Molecule Level, *Angew. Chem.*, 2021, **133**, 13051–13058.

32 V. T. Mai, V. Ahmad, M. Mamada, T. Fukunaga, A. Shukla, J. Sobus, G. Krishnan, E. G. Moore, G. G. Andersson and C. Adachi, Solid cyclooctatetraene-based triplet quencher demonstrating excellent suppression of singlet–triplet annihilation in optical and electrical excitation, *Nat. Commun.*, 2020, **11**, 5623.

33 *C. Z. M. GmbH, Zen 3.0 SR (black) (64 bit), 1997–2024, ZEN*, 2012.

34 *I. The MathWorks, Matlab R2022a Update 3 64-bit (win64)*, 2022, R2022a.

35 *N. OriginLab Corporation., OriginPro 2021 (Academic)*, MA, USA, 2021, 2021.